Acta Materialia 167 (2019) 40–50

Contents lists available at ScienceDirect

Acta Materialia

journal homepage: www.elsevier.com/locate/actamat

Full length article

Three-dimensional observations of grain volume changes during annealing of polycrystalline Ni

Aditi Bhattacharya [a], Yu-Feng Shen [b], Christopher M. Hefferan [b, 1], Shiu Fai Li [b], Jonathan Lind [b, 2], Robert M. Suter [b], Gregory S. Rohrer [a, *]

[a] Department of Materials Science and Engineering, Carnegie Mellon University, Pittsburgh, PA, 15213, USA
[b] Department of Physics, Carnegie Mellon University, Pittsburgh, PA, 15213, USA

ARTICLE INFO

Article history:
Received 13 November 2018
Received in revised form
9 January 2019
Accepted 14 January 2019
Available online 21 January 2019

ABSTRACT

The orientations, locations, and sizes of approximately 2500 grains in a Ni polycrystal were measured at six points in time during an interrupted annealing experiment by synchrotron x-ray based, near field high-energy diffraction microscopy. The volume changes were compared to the geometric characteristics of the grains in both the original microstructures and microstructures in which adjacent twin related domains were merged. Neither the size of a grain nor the number of its nearest neighbors correlates strongly to a grain's volume change over the time scale of this experiment. However, the difference between the number of neighbors a grain has, *F*, and the average number of neighbors of the neighboring grains have, $\langle F_{NN} \rangle$, is correlated to the volume change. A grain with more (fewer) neighbors than $\langle F_{NN} \rangle$ usually grows (shrinks). The correlation between the volume change and $F - \langle F_{NN} \rangle$ is obvious only if adjacent twin related domains are merged. The correct sign of the volume change is predicted by $F - \langle F_{NN} \rangle$ about two thirds of the time. The results show that the volume change for a given grain is better predicted by comparing a grain's characteristics to its neighbor's characteristics than to the characteristics of the entire ensemble of grains.

1. Introduction

Annealing a polycrystalline material at high temperature leads to grain growth, during which some grains shrink and are eliminated and the average grain size increases [1–3]. While it may be argued that changes in the average grain size and grain size distribution with time are relatively well understood, we know much less about the behavior of individual grains in this process and what factors control whether a specific grain shrinks or grows. The earliest studies that focused on individual grains were quasi two-dimensional and used soap froths or polycrystalline succinonitrile as proxies for inorganic microstructures because their transparency made it possible to make dynamic observations. For example, Smith [4] examined the growth of cells in a two-dimensional soap froth formed in a small flat glass cell and remarked upon the positive correlation between a cell's size and its number of near neighbors. Palmer et al. [5] verified the Mullins-Von Neumann "N-6" rule [6] by observing grain growth in succinonitrile. It was recognized that grain growth occurred to eliminate excess energy while also balancing topological requirements for space-filling and local interfacial equilibrium at triple junctions [7,8].

In 1970, Aboav [9] recognized empirically that grains in 2D sections were arranged such that the number of neighbors of a grain (*F*) is related to the average number of neighbors of the neighboring grains, $\langle F_{NN} \rangle = 5 + 8/F$. This eventually resulted, after some theoretical advancements, in what is now known as the Aboav-Weaire (AW) [10,11] law:

$$\langle F_{NN} \rangle = (\overline{F} - 1) + \frac{(\overline{F} + \mu_2)}{F} \quad (1)$$

where $\overline{F}$ is the average number of neighbors and μ_2 is second moment of the distribution of grain nearest neighbors (faces).

* Corresponding author.
E-mail addresses: aditib@andrew.cmu.edu (A. Bhattacharya), yufengs@andrew.cmu.edu (Y.-F. Shen), chefferan@rjleegroup.com (C.M. Hefferan), shiu.fai.li@gmail.com (S.F. Li), lind9@llnl.gov (J. Lind), suter@andrew.cmu.edu (R.M. Suter), rohrer@cmu.edu (G.S. Rohrer).
[1] Current affiliation: RJ Lee Group, 350 Hochberg Rd., Monroeville, PA 15146, USA.
[2] Current affiliation: Materials Engineering Division, Lawrence Livermore National, Laboratory, 7000 East Ave., Livermore, CA 94551, USA.

https://doi.org/10.1016/j.actamat.2019.01.022
1359-6454/

Noting that 3D microstructure studies find a strong positive correlation between F and the grain size [12–15], one can interpret the AW law as simply saying that large grains (those with many neighbors) are on average surrounded small grains (those with fewer neighbors) and vice versa. In the context of grain growth, the AW law emphasizes that the size and shape of a grain is related to its neighbors and it has successfully described different kinds of cellular patterns [11] in steady state and transient structures [16].

The first extensive observations of three-dimensional (3D) grain growth dynamics were produced by computer simulations, which assumed isotropic grain boundary properties. 3D grain growth simulations using the Monte Carlo Potts model [17], boundary tracking methods [18], the vertex method [18], and the phase field method [19] make it possible to study isotropic grain boundary motion in three dimensions. These studies verified the idea that the distribution of grain sizes normalized by mean grain size was time invariant during normal grain growth. Those studies that compared $\langle F_{NN} \rangle$ and F for the simulated 3D structures found a functional relationship consistent with the AW law [17,18].

While computer models have been used to simulate 3D microstructural evolution during grain growth, experiments have been more difficult. Studies of static 3D microstructures that have measured grain boundary curvature (assumed to be related to grain boundary velocity) have provided some information on the relation between topology and grain boundary kinetics [13,20]. For example, using data from the shapes of 2098 β-Ti grains, the relation between F and $\langle F_{NN} \rangle$ in 3D was consistent with the AW law [13]. Also, the integral mean curvature of grain faces was linearly related to F - $\langle F_{NN} \rangle$, with zero integral mean curvature corresponding to F - $\langle F_{NN} \rangle$ equal to zero, illustrating the importance of neighboring grains on the curvature of a grain face and whether or not its motion will increase or decrease the volume of the grain [13]. Similar findings were reported for an austenitic steel [20]. While the observed correlation between the integral mean curvatures and F - $\langle F_{NN} \rangle$ is significant, it remains to be seen if actual volume changes with time are correlated to F - $\langle F_{NN} \rangle$; one of the main goals of this paper is to test this idea.

The recent development of synchrotron x-ray based, near-field High Energy X-ray diffraction microscopy (nf-HEDM) [21] and diffraction contrast tomography (DCT) [22] make it possible to track the evolution of three-dimensional microstructures while they respond to external stimuli. For example, the response of a high purity Al polycrystal to annealing was measured by nf-HEDM [23]. The nondestructive nature of the orientation mapping made it possible to observe the growth of new grains and verify the salient features of microstructure recovery and recrystallization. This same technique was used to observe the effect of the tensile strain on the microstructural evolution of polycrystalline copper [24] and the formation of twins in polycrystalline Ni [25] and Zr [26]. McKenna et al. [27] compared the morphology of grains of β-Ti measured by DCT, before and after annealing, to morphologies predicted by a phase-field simulation assuming isotropic grain boundary properties. They reported good agreement between the simulated and observed microstructures in some regions of the microstructure. DCT has also been been used to track individual crystals during grain growth in Fe [28] and measure grain rotations during coarsening in a semi-solid Al-Cu alloy [29]. The most detailed study of the evolution of grain sizes and shapes is a recent report by Zhang et al. [30] on grain growth in polycrystalline Fe. They found that while the MacPherson-Srolovitz theory [31] for grain growth accounted well for the average geometric characteristics of the microstructure, individual grains often behaved differently.

The goal of this work was to determine which characteristics of grains in an initial state best predict the sign of the volume change after some grain growth has occurred. To do this, an algorithm was developed to track each grain across all the anneal states. The volume changes of the grains were compared to factors such as initial volume, the number of contacting neighbors (F), and the average number of neighbors of the neighboring grains, $\langle F_{NN} \rangle$. The results lead to the conclusions that while the size and number of neighbors are not well correlated to the volume change, the quantity F - $\langle F_{NN} \rangle$ is correlated to the volume change of the grains, but with two important stipulations. The first is that the correlation is strongest when adjacent twin related domains were merged and treated as a single grain [28]. The second is that the volume change and F - $\langle F_{NN} \rangle$ are correlated only on average, while some individual grains behave differently.

2. Methods

High purity polycrystalline nickel was obtained from Alfa Aesar in the form of a 1 mm diameter nickel wire. The sample was annealed sequentially in a reducing atmosphere (97% N_2, 3% H_2) at 800 °C, for approximately 30 min, five different times. After each anneal stage, the sample was cooled to room temperature and the 3D microstructure was measured (details of the anneals are listed in Table 1). After each annealing interval, nf-HEDM was used to create 3D orientation maps of the microstructure utilizing the 1-ID beam line at Argonne National Laboratory's Advanced Photon Source. The details of this data collection have been reported previously [32] and preliminary analyses are contained in two Ph.D. theses [33,34]. Of importance to the current work, the volume of materials characterized contained approximately 2500 grains, the x-y plane was discretized into 600×600 voxels with lateral dimensions of 2.3 μm, the vertical separation of the x-y planes is 4 μm, and each volume contains at least 70 x-y planes.

The three-dimensional Ni microstructure was reconstructed from nf-HEDM data using the IceNine implementation of the forward model method [35]. The result is a file that discretizes the microstructure into parallel 2D layers made up of equilateral triangles. For each triangle, the spatial coordinates, the Euler angles in the Bunge convention, and a confidence index, C, reflecting the reliability of the orientation determination, are specified. An in-house program was used to convert this information to $2\ \mu m \times 2\ \mu m$ square pixels in each layer that could be directly read by DREAM.3D [36].

2.1. 3D reconstruction and grain segmentation

The sequence of steps for creating a 3D grain structure in DREAM.3D was similar to the default pipelines used to generate 3D orientation maps from focused ion beam serial sectioning experiments [14]. Briefly, the procedure begins by applying a threshold on C to generate a Boolean mask that distinguishes high and low confidence voxels. The individual sections are then laterally aligned by minimizing the layer-to-layer misorientation using only the high confidence data. The lateral shifts required for alignment ranged

Table 1
Summary of annealing parameters.

Anneal State	Duration (min)	Temperature (°C)
0	120	750
1	23	800
2	30	800
3	25	800
4	35	800
5	25	800

from 0 to a few voxels. After alignment, the microstructure is represented by three-dimensional voxels with dimensions of 2 μm × 2 μm×4 μm. So-called clean-up procedures are then used to assign orientations to low confidence voxels using information from surrounding high confidence voxels. The data are then segmented into grains by grouping sets of contiguous voxels with small relative misorientations. In this procedure, there were two threshold parameters that influenced the results. One was the minimum number of voxels that are considered to reliably reflect the volume of a grain. A test of the sensitivity of the results to this parameter is summarized in Fig. 1. Based on this, the minimum accepted grain size was set to be 3^3 or 27 voxels because this was the first integer cubed beyond which the average grain size and number of grains changed only slowly. The second threshold parameter was the minimum disorientation for segmenting voxels into grains. This was set at 2° because the typical orientation difference between the same grain in two successive anneal states was less than 2°.

After the grain segmentation, each anneal state had approximately 2500 grains, two-thirds of which are bulk grains and the others are surface grains (grains that contact the exterior volume of the sample or the vertical limits of the field of view are referred to as surface grains, the remainder are referred to as bulk). The average equivalent spherical grain radius in the first anneal state (denoted 0) is 19 μm. This increased at each anneal state to 23 μm in the final anneal state (denoted 5). There are numerous challenges in identifying the same grains in successive anneal states. First, the volume imaged in each anneal is not exactly the same (see Fig. S1). The intent was to slightly increase the volume measured so as to minimize the loss of internal grains as growth took place; however beamtime limitations prevented a uniform increase. Therefore, there are grains in the field of view after one anneal state that might not have been in the previous field or the next one. Second, a grain that is classified as a bulk grain in one state may impinge with a surface in another state and have a different volume and centroid location. Third, some grains will shrink and disappear in the course of the experiment, so it will not be possible to track them throughout the entire annealing sequence.

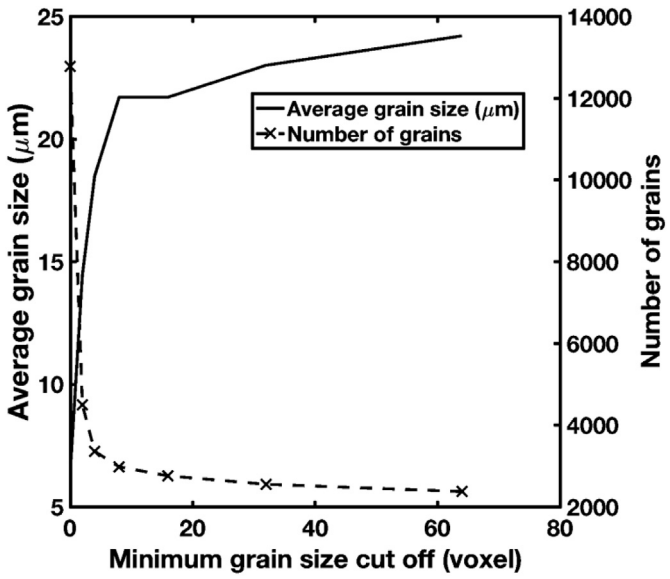

Fig. 1. Changes in the average grain size and number of grains in the reconstruction depends on the minimum size cut off during grain segmentation. The data are from anneal state 5 and are characteristic of other anneal states.

2.2. Grain matching algorithm

An algorithm was developed to adapt to these challenges. From each of the reconstructed microstructures, a list of all grains was constructed which included the grain's centroid location (coordinates) and the orientation (Euler angles). As a first step, grains in successive anneal states with similar orientations and locations were identified and the distribution of their misorientations and separations were determined (see Fig. 2a and 2b). Note in Fig. 2b that the distribution of separations reaches maximum at about 20 μm. This is assumed to be a rigid translation associated with aligning the samples after the heat treatment. The three components of the translation vector were obtained separately (see Fig. S2) and this vector was subtracted from the coordinates of the voxels in the second state to improve the alignment. After this procedure, the average difference in the locations of the centroids was nearly zero. Similar rigid translations were applied to all anneal states.

A kernel approach was used to identify the same grain in sequential anneal states. For each grain in the first anneal state, the distances to all grains in the next anneal state were calculated. Next, the disorientation between each grain from the first anneal state and every grain in the next anneal state whose centroid was less than five times the grain radius from the centroid of the grain in the first anneal state was calculated. These values were stored in a matrix that contained the disorientation and centroid distance of every grain in first state with respect to a neighborhood kernel of grains in the second state. To identify the same grain in sequential anneal states, we assumed that grains with similar locations and orientations were the same. To perform this match quantitatively, we defined a confidence index (CI) to measure the likelihood that two grains match:

$$CI_{ij} = C_1 \Delta g_{i,j} + C_2 \Delta L_{i,j} \tag{2}$$

where $\Delta g_{i,j}$ is the disorientation between grains i and j, $\Delta L_{i,j}$ is the distance between the centroids of grains i and j, and C_1 and C_2 are constants to scale the parameters so that disorientation and position had similar weights in determining CI_{ij}. Typical values were $C_1 = 0.2\ (^\circ)^{-1}$ and $C_2 = 0.005\ \mu m^{-1}$.

A grain in the first anneal state is then matched with the grain in the second anneal state that has the lowest value of CI. The algorithm was tested by comparing duplicate microstructures and in these cases, 100% of the grains were matched appropriately. The algorithm was further tested by using the initial structure as the starting point for a 3D grain growth simulation. The phase field simulation was run until the average volume change was 15%; the matching algorithm found all of the pairs except for the grains that disappeared. When the algorithm is used on real data, multiple grains in the first anneal state were occasionally matched to the same grain in the second anneal state. In these cases, the grain pair with the lowest CI was selected as the true match and the others were classified as unmatched. This problem is related to multiple twinning, which creates grains with the same orientation in close proximity. Pseudo-code for the matching algorithm is provided in Fig. S3. A schematic illustration of the process is illustrated in Fig. 3. For grain 92 in the first state, CI is computed for all grains whose centroids are separated from grain 92's centroid by less than five times the radius. Because grain 2743 in the second state had the lowest CI, it is assumed to be grain 92 in the second state. A visual comparison of Fig. 3c and 3d confirms that the two grains are the same.

When matching grains in different anneal states with real data, it is not possible to match all observed grains. One of the most significant problems is that the field of view at each time step is not

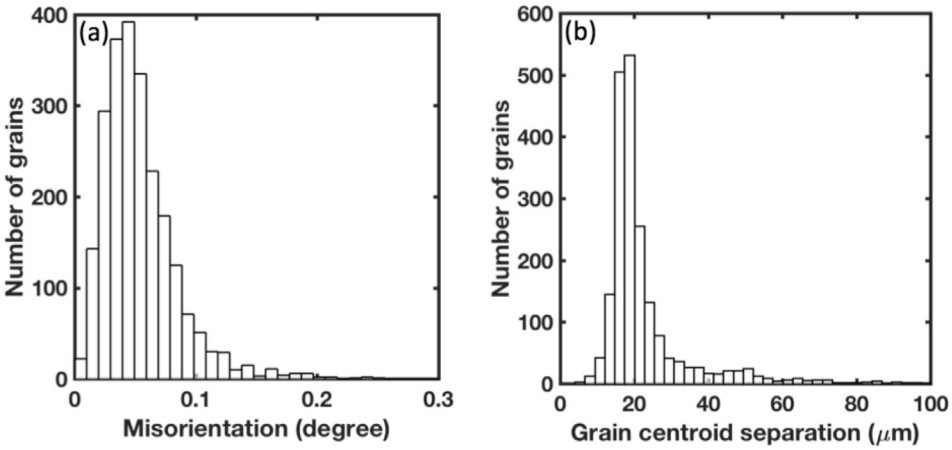

Fig. 2. Distributions of (a) misorientations, (b) centroid separations between matched grain pairs. (b) shows that most grains are offset by about 20 μm.

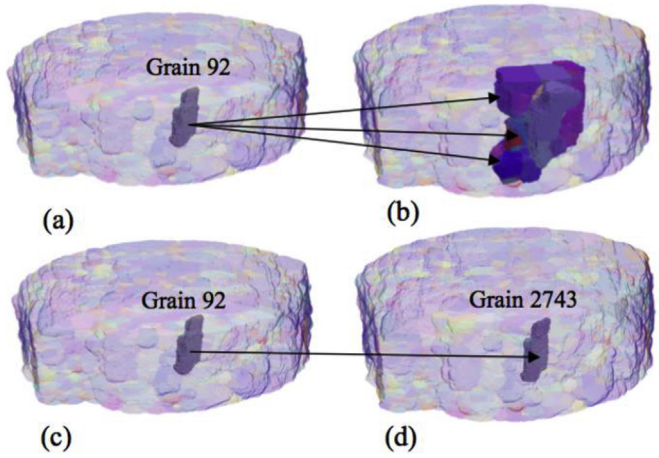

Fig. 3. Schematic illustration of the grain-tracking algorithm. (a) Grain 92 in the initial state is considered, all other grains are displayed as semi-transparent. (b) In the next state, all grains within five grain radii of Grain 92's centroid are considered candidates and displayed as opaque. (c & d). After computing the CI for all candidate grains, Grain 2743 in the next state has the minimum CI and is matched to Grain 92 in the initial state. The sample diameter is 1 mm.

exactly the same and if a grain is not included in both 3D images, it is not possible to match. For example, the image in Fig. 4 shows anneal state 4, where the unmatched grains are opaque and the matched grains are transparent. In addition to some small bulk grains (these are grains that shrank and disappeared), there is a large aggregate of grains at the lower boundary of the sample that were not matched because they were outside the field of view of

Fig. 4. The sample after anneal state 4. Grains that matched are displayed semi-transparent and unmatched grains opaque. The unmatched grains at the bottom did not overlap with the field of view of the next state and could not be matched. The sample diameter is 1 mm.

the next set of data. All six fields of view are shown for comparison in Fig. S1. The next problem is that small grains can disappear (or shrink to smaller than the segmentation threshold) and cannot be matched in the next time step. For real data, the matching efficiency (matched grains/total grains) was 88%, which accounted for an average of 97% of the volume of the microstructure (see Fig. 5). The matching was implemented both with time (states 0 to 5) and in reverse time (states 5 to 0) and the results were comparable.

The tracking program was also run with the condition that only bulk grains were considered. In this case, the average matching efficiency falls to 81%. The reduced efficiency is because some grains within the bulk in one state may, in the next state, impinge on a surface either because they grew and intersected the surface or because of a change in the field of view.

From the images of the microstructure in Fig. S1, it is obvious the microstructure is twinned, as expected for Ni. In fact, in the final anneal state, grain boundaries with the twin misorientation (60° misorientation about [111]) make up 29% of all grain boundary area. Because twins have odd shapes [37] and twin boundaries have unusually low mobilities [38], it is not clear how they influence the grain growth process. To minimize the influence of twins, we transformed the twinned microstructure to a more equiaxed microstructure by combining into a single grain all grains that share a grain boundary with the twin misorientation. This was implemented using the "merge twins" filter in DREAM.3D [36,39]. After merging the twins, there were fewer grains. For example, in the initial state, 2972 grains were merged to 926 grains. Examples of the microstructure before and after the twins were merged are illustrated in Fig. S4. The grain-matching algorithm had to be modified to match the twin related domains. Specifically, it was necessary to preserve the characteristics (orientation and centroid location) of all the grains merged into a single twin related domain in each state, and compare these groups to match the merged grains.

3. Results

The initial and final reconstructed volumes are illustrated in Fig. 6. Note that grain visualizations shown in this paper show the sets of voxels (as described above) with no smoothing applied. The results discussed here do not require smoothing. Comparing the two, the average grain size in the final anneal state is noticeably larger than in the initial state. Note that there is a difference in the field of view; a larger volume was mapped in the final anneal state than in the initial anneal state. While significant changes occurred during annealing, it is still possible to identify some common grains

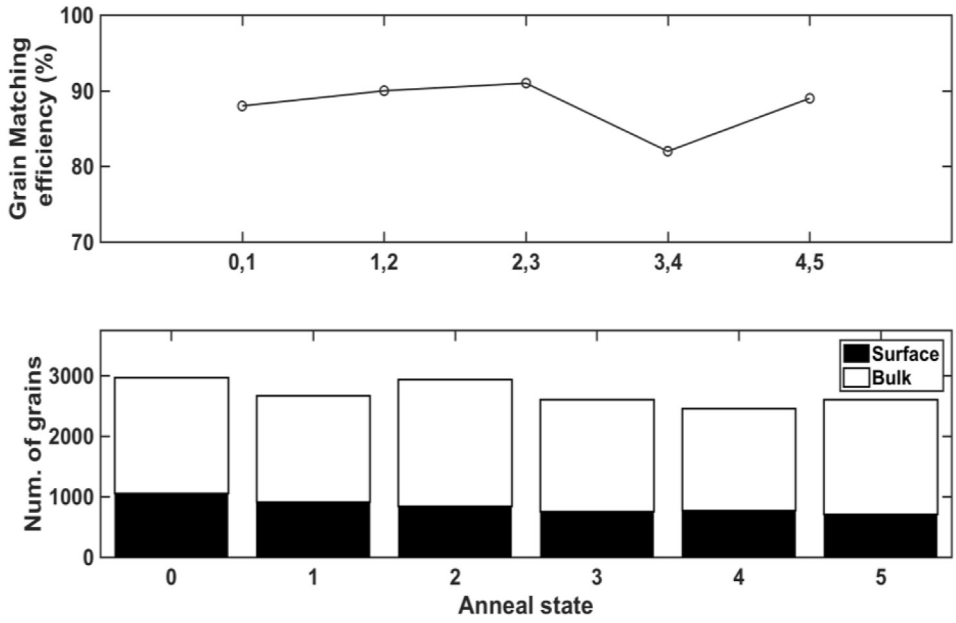

Fig. 5. (a) Grain matching efficiency between the anneal states. (b) Distribution of number of bulk and surface grains in each state.

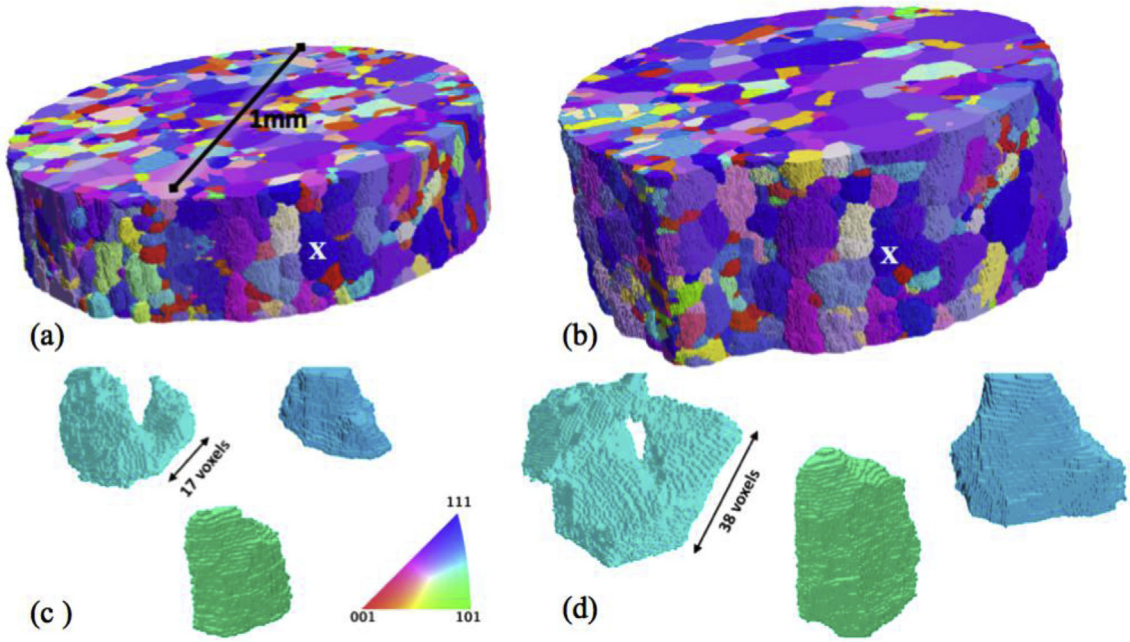

Fig. 6. Visualizations of the microstructures in the (a) initial and (b) final anneal states. The grains are colored by orientation with respect to the cylinder axis, according to the inset color key. One example of a matching surface grain in the two states is marked with a white "X". Three selected grains in the initial anneal state are illustrated in (c) and the grains they are matched to in the final anneal state are shown in (d). (For interpretation of the references to color in this figure legend, the reader is referred to the Web version of this article.)

on the periphery of the sample, such as the one marked with a white X; all six reconstructed volumes are illustrated in Fig. S1. A comparison of three matched grains in the initial and final anneal states (Fig. 6c and d) shows that they have the same orientation (color) and similar shapes. The three individual grains that are illustrated all increased in volume. Two are relatively equiaxed but the other has a 'U' shape in the initial state and has a tunnel through it in the final state. Because of extensive twinning in the microstructure, this shape is not unexpected. The grain within the tunnel is a twin.

To demonstrate the effectiveness of the grain tracking algorithm, many individual grains were visualized in each anneal state. Fig. 7 illustrates a grain that started small, but grew during annealing. The growth rate was clearly different during different annealing periods. For example, it grew dramatically between (b) and (c). Similarly, Fig. 8 is a visualization of a grain that shrank during annealing. In the final state (5), the grain could not be detected, suggesting that it shrank below the 27 voxel threshold used in the grain segmentation.

1800 grains were identified that matched in all five anneal

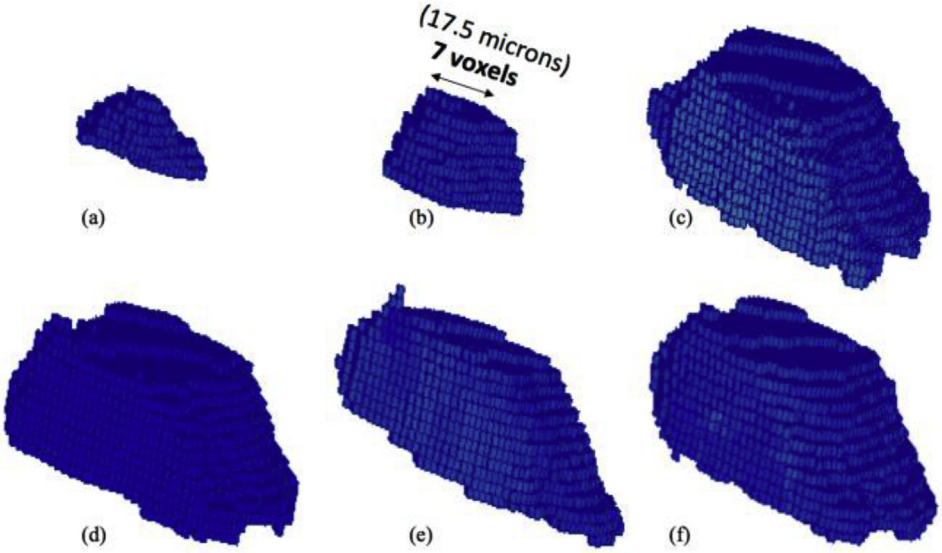

Fig. 7. Visualization of a growing grain in each anneal state. a) 0, b) 1, c) 2, d) 3, e) 4, f) 5.

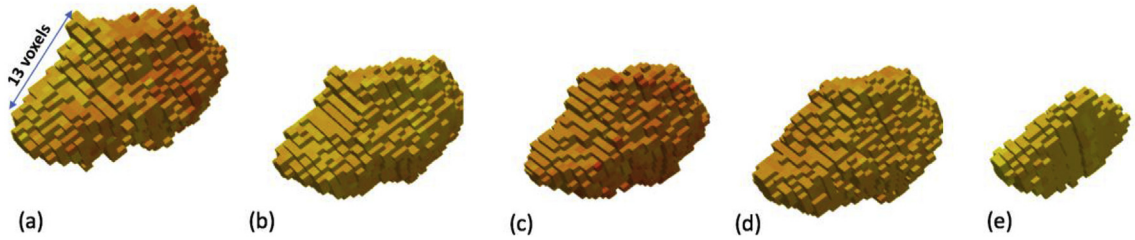

Fig. 8. Visualization of a shrinking grain in the first five anneal states. a) 0, b) 1, c) 2, d) 3, e) 4.

states. While this is less than the total number of grains, it is limited by the condition that the grain had to appear in all five anneal states. Grains that shrank below the minimum detectable grain size (such as the one illustrated in Fig. 8) are not counted. The greatest percentage fractional change in grain radius amongst these grains (between the initial and final anneal states) was 965%. It should be noted that the surface grains at the top and bottom of the measured volume do not provide reliable measures of the volume change; a small change in the field of view can dramatically change the measured volume of a grain. Concentrating on only those grains that did not touch the surface of the volume in any state, and that matched in all states, eliminates this artifact, but creates other artifacts. For example, this selection criteria is biased against the largest grains (those that intersect the surface in some state) and smallest grains (those that disappear during the experiment). Accepting these limitations, there are 701 bulk grains that appeared in all anneal states; 330 grains grew while the remainder (371) shrank. This distribution is shown in Fig. 9 and illustrates that almost 80% of the grains have small volume changes during the experiment (less than $\pm$ 20%).

As expected, the average grain size increases during annealing. Fig. 10 shows the average grain radius in each anneal state, using grains selected by various conditions. When all grains in the reconstructed microstructure are considered, the average spherical equivalent grain radius increases from 19 μm to 23 μm. The surface and bulk grains behave the same way, but the surface grains are larger than average and the bulk grains are smaller than average. For surface grains that meet the upper and lower boundaries, where the microstructure is terminated by the limits to the field of

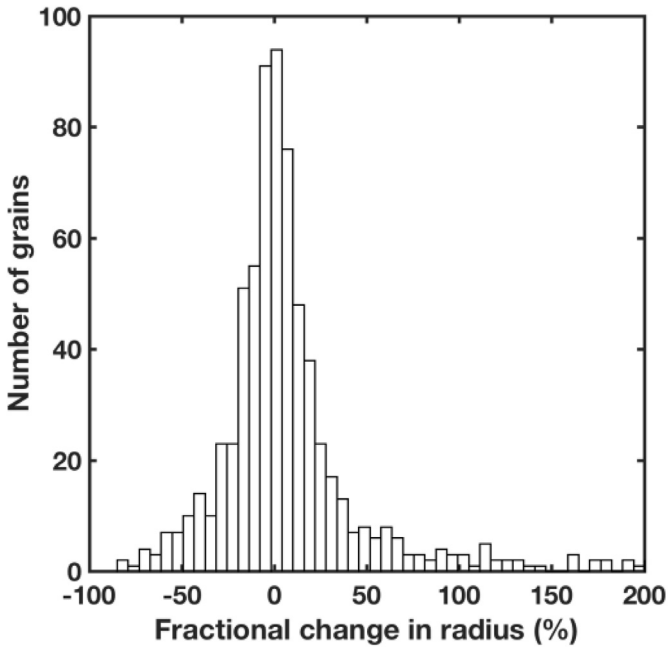

Fig. 9. Histogram of fractional changes in the grain radii. This is the fractional change in radius from the initial to final state, for 701 grains present in all six states in the twinned microstructure that did not contact the surface of the measured volume.

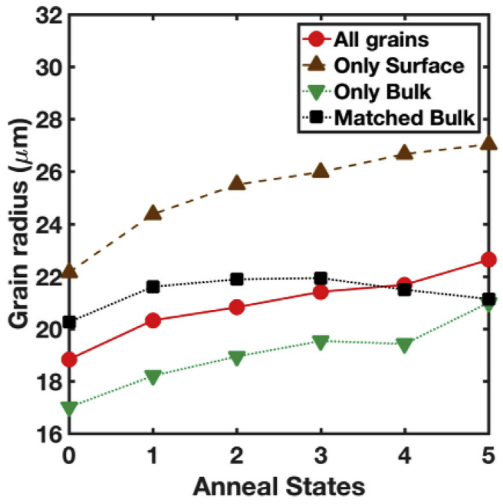

Fig. 10. Average grain radius in each state for all grains (circles) and for selected subsets.

view, the surface grains are larger on average because the probability that a grain intersects the surface is proportional to its size. For the lateral surfaces, there is also a contribution from the tendency of the grain boundaries to intersect the free surface at close to 90°, which can increase boundary curvature and lead to the preferential growth of surface grains. We did not attempt to distinguish between these two phenomena. Those grains that do not contact the surface and are tracked in each anneal state have a roughly constant grain size. These are the grains that were not small enough to shrink and disappear during the experiment nor were they so large that they impinged with the surface as a result of growth or a shift in the field of view. The normalized grain size distributions before and after merging twins are illustrated in Fig. S5 and the distributions of faces per grain (F) before and after merging twins are illustrated in Fig. S6. In each case, the distributions appear self-similar throughout the experiment.

The changes illustrated in Fig. 10 are the sum of contributions from hundreds of grains. The behaviors of individual grains are not as regular. To illustrate examples of how individual grains change size over time, the spherical equivalent grain radii of six grains in each anneal state are illustrated in Fig. 11. Grain 1 initially increased in size, and then shrank, from 43 μm to 33 μm. Grain 2 increases, decreases, and increases again. Other grains changed continuously, such as Grain 6, which grew from a radius of 25 μm to 38 μm.

The results were compared to the AW law to determine if the number of neighbors that a grain has is correlated to characteristics of the neighboring grains. Rearranging Eq. (1), we find a relation between $\langle F_{NN}\rangle F$ as a function of F:

$$\langle F_{NN}\rangle F = (\overline{F}-1)F + (\overline{F}+\mu_2) \tag{3}$$

The data in Fig. 12, which includes all grains in the twinned microstructure, shows good agreement with Eq. (3), where $\overline{F} = 16$ and $\mu_2 = 21$. The actual values of $\overline{F}$ and μ_2 measured from the data are $\overline{F} = 12$ and $\mu_2 = 78$. While the fit to Eq. (3) is good, the resulting parameters ($\overline{F}$ and μ_2) do not correspond to the observed values. We do not currently have an explanation for this discrepancy, but it does bring into question the application of the AW law to three-dimensional data.

In Hillert's [40] classical mean field theory of grain growth, it is assumed that there is a critical grain size above which grains (on average) grow and below which they shrink. However, when the volume change of a grain is considered as a function of the initial grain radius, the two quantities do not appear to be strongly correlated. The data are shown in Fig. 13, where grains were binned according to their radii and the mean (square) and standard deviations (bars) are plotted for each grain size. Volume changes in the twinned microstructure (Fig. 13a) appear independent of grain size. In the microstructure with merged twins (Fig. 13b), the three largest positive volume changes occur for the three largest grain size categories (approximately twice the mean size), but at smaller sizes the volume change is independent of size.

Some grain growth theories have suggested that there is a critical number of neighbors above which grains grow and below which they shrink [41,42]. In fact, a grain's size and number of neighbors are strongly correlated such that larger (smaller) grains typically have more (fewer) neighbors, as shown in Fig. S7. This is a consequence of the cooperative process of grain growth. In Fig. 14, the grains were grouped by their number of neighbors and the mean (squares) and standard deviation (bars) of the volume change in each category is plotted. For the twinned microstructure (Fig. 14a), F is a poor predictor of whether a grain will shrink or grow. For the microstructure after the twins have been merged, there is some evidence that grains with more sides are more likely

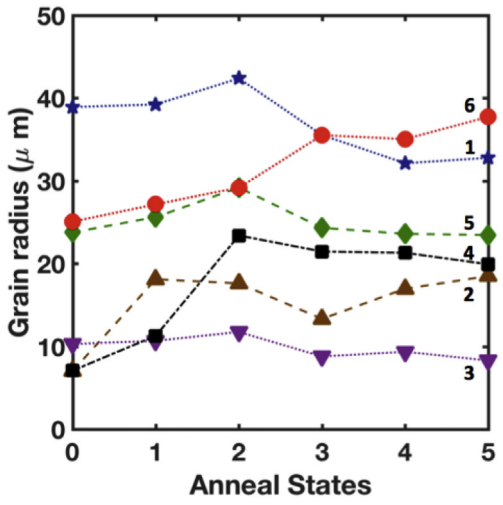

Fig. 11. Grain radii at six anneal states for six representative grains.

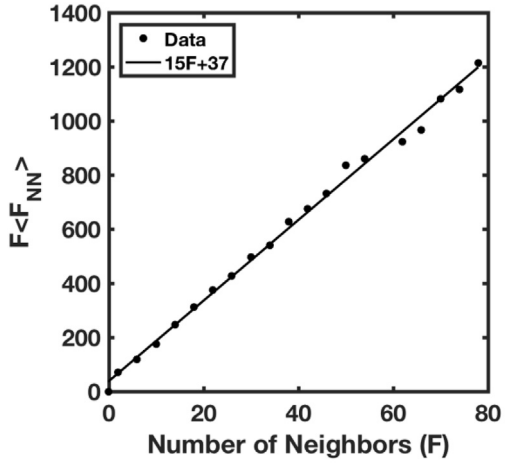

Fig. 12. The product of the number of near neighbors (F) and the average number of nearest neighbors of the neighbors ($<F_{NN}>$) plotted versus the number of neighbors (F). The line is a fit to the AW law.

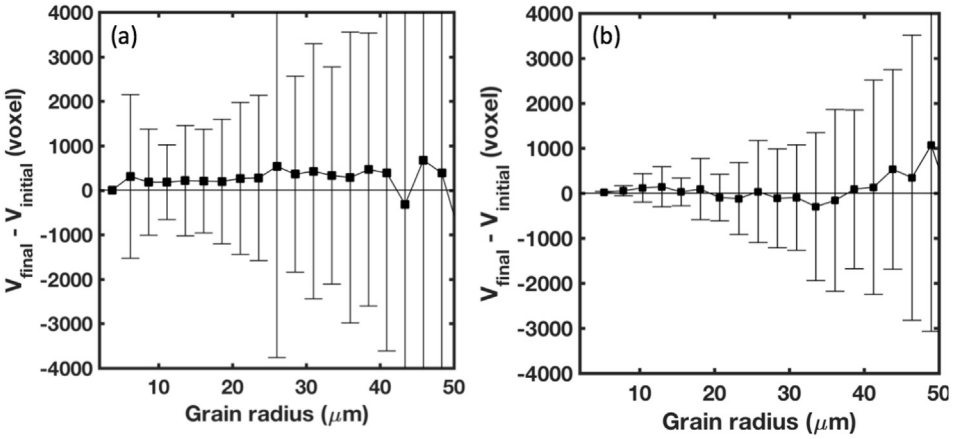

Fig. 13. Change in volume versus initial grain size for all anneal states for (a) the twinned microstructure and (b) after merging twins. For each grain radius class, the marker is the mean value and the bar shows one standard deviation of the distribution.

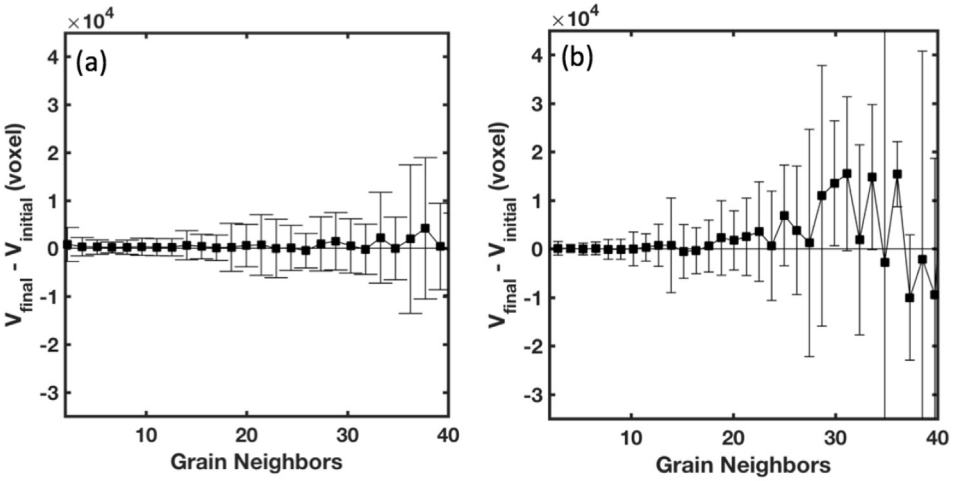

Fig. 14. Change in volume versus initial number of grain neighbors for (a) the twinned microstructure and (b) after merging twins. For each class of F, the marker is the mean value and the bar shows one standard deviation of the distribution.

to grow. Grains with more than 18 sides have positive mean volume changes, except for four categories among the five with the largest number of sides.

It has been shown by Von Neumann and Mullins [6,43] that when local mean curvature drives grain boundary motion, the total volumetric growth rate (dV/dt) is given by Eq. 4:

$$\frac{dV}{dt} = V^{1/3} M \gamma \mathscr{g} \tag{4}$$

where M is the grain boundary mobility, γ is the excess interfacial energy per unit area, and $\mathscr{g}$ is the normalized integral mean curvature of the grain faces. Integrating Eq. 4, we get:

$$\Delta V^{2/3} = \frac{2}{3} \int M \gamma \mathscr{g} \, dt \tag{5}$$

It has been observed experimentally that $\mathscr{g}$, the normalized integral mean curvature, is linearly proportional to F - $\langle F_{NN} \rangle$ [13,20]. Using this relation, we approximate Eq. 5 in the following way:

$$\Delta V^{2/3} = V_f^{2/3} - V_i^{2/3} \propto \int (F - \langle F_{NN} \rangle) \, dt \approx (F - \langle F_{NN} \rangle) \, \Delta t \tag{6}$$

where V_f and V_i are the final and initial volumes, respectively. This suggests that in a given period of time (Δt), grains that have more (fewer) faces than the average of their neighbors should grow (shrink).

The data in Fig. 15 show the relationship between $\Delta V^{2/3}$ and $F - \langle F_{NN} \rangle$ for all grains (a) and after merging the twins (b). In each plot, the marker shows the mean value in each class and the bar indicates the standard deviation. Volume changes in the twinned microstructure (Fig. 14a) appear almost independent of $F - \langle F_{NN} \rangle$. When the twins are merged, the correlation between $\Delta V^{2/3}$ and $F - \langle F_{NN} \rangle$ is much stronger. In this case, all positive mean values of $F - \langle F_{NN} \rangle$ are associated with positive values of $\Delta V^{2/3}$. The average volume changes for grains with negative $F - \langle F_{NN} \rangle$ are generally negative, but not strongly negative. This is likely to be due, in part, to the fact that when small grains shrink below the detection limit, they are no longer tracked and these negative volume changes are not included. While it is possible to include these assumed negative volume changes, it is difficult to discern if a grain is not tracked because it actually disappeared or if it is no longer in the field of view. It should be noted that while the mean values follow the expected trend, the width of the distribution about the mean is large. Therefore, a positive or negative value of $F - \langle F_{NN} \rangle$ is not an absolute predictor of the sign of the volume change. However, the sign of $F - \langle F_{NN} \rangle$ predicts the sign of the volume change in 65% of the grains.

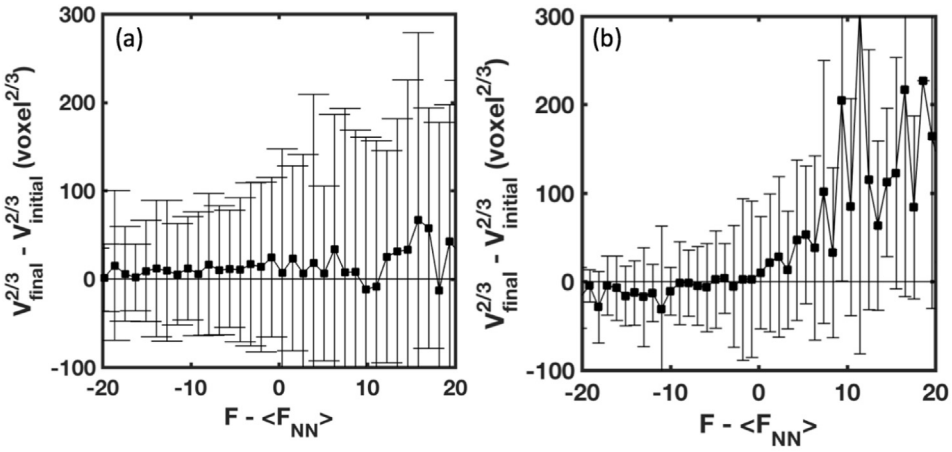

Fig. 15. Change in volume versus the difference between the number of neighbors and the average number of neighbors of the neighbors in (a) the twinned microstructure and (b) after merging twins. For each class of $F-\langle F_{NN}\rangle$, the marker is the mean value and the bar shows one standard deviation of the distribution.

Note that all grains, including surface grains, were included in this analysis. This clearly introduces errors, but some of the errors compensate. For example, a surface grain does not have its full complement of near neighbors, so F is reduced from the true value. However, most of the neighboring grains face a similar restriction, so $\langle F_{NN}\rangle$ is similarly reduced. In an ideal situation, these grains could be excluded or included according to the criterion introduced by Rowenhorst [13]. Rowenhorst argued that grains whose centers of mass are less than 2<R> from the boundary of the volume should be eliminated, where <R> is the mean grain radius. Unfortunately, when this criterion is applied to our data, there are so few grains remaining that there is insufficient data for the analysis, especially for the sample where the twins were merged. If we relax Rowenhorst's criterion and remove grains whose centers of mass are less than <R> from the boundary of the volume, more than half of all grains are removed, but 300 to 400 grains remain in each anneal state. The correlation between the volume change and $F-\langle F_{NN}\rangle$ for this more selective data is illustrated in Fig. S8. While the result is certainly noisier than Fig. 15, because there are fewer grains, the results are consistent with the trends in Fig. 15. In other words, the comparison of Fig. 15 and Fig. S8 suggests that eliminating grains near the surface does not change the conclusion that grains with positive mean values of $F-\langle F_{NN}\rangle$ are associated with positive values of $\Delta V^{2/3}$.

4. Discussion

Synchrotron x-ray based, near field High Energy Diffraction Microscopy (HEDM) makes it possible to measure the shapes and volumes of grains within a solid at different time intervals during interrupted annealing. Using these data, it is possible to determine which grains increased in volume and which grains decreased in volume and compare the volume changes to the characteristics of the grains in the initial state. The results do not support the idea that there is critical size, or a critical number of near neighbors, above which a grain grows and below which a grain shrinks. Instead, mean values of the volume change are correlated to $F-\langle F_{NN}\rangle$. It should be noted that the grain size, R, and its number of nearest neighbors, F, are strongly correlated with one another (see Fig. S7). Therefore, it should also be true that volume changes are correlated to $R-\langle R_{NN}\rangle$, where $\langle R_{NN}\rangle$ is the average radius of the nearest neighbor grains. The correlation between $R-\langle R_{NN}\rangle$ and the volume change is illustrated in Fig. S9 and, while having more noise, shows the same trend as Fig. 15. It should also be mentioned that a recent study of α-Fe also found a correlation between the volume change and $F-\langle F_{NN}\rangle$ [44].

In retrospect, it is naïve to think that the size of a grain, compared the ensemble average grain size, determines whether it grows or shrinks. A specific grain grows or shrinks by exchanging mass with its neighbors. During a small increment of time, a specific grain has no information about ensemble averages and is only influenced only by its nearest neighbors. So, it is a comparison between the characteristics (F, R) of the grain of interest with the characteristics of its immediate neighborhood ($\langle F_{NN}\rangle$, $\langle R_{NN}\rangle$) that determines whether it grows or shrinks. In other words, for a grain to grow (shrink), it is less important that a grain be larger (smaller) than the average grain size than it is for a grain to larger (smaller) than its neighbors.

While the mean values of the volume change are correlated to $F-\langle F_{NN}\rangle$, as illustrated in Fig. 15, there are many exceptions which are apparent in the distributions about the mean values. On a grain-by-grain basis, ΔV and $F-\langle F_{NN}\rangle$ have the same sign 65% of the time. Among the other 35%, some are certainly linked to limitations in the data. One source of error arises when the volume change is very small. As illustrated by Fig. 9, most grains have small volume changes and small differences in the reconstruction may change the sign of the volume change. Another source of error is that grains that disappear are not included in the statistics and this artificially reduces the mean volume change of shrinking grains. The free surfaces of the volume are also obvious sources of error. When some of the largest outliers in the distribution were visualized, they were almost always caused by erroneous volume changes in grains at the upper and lower limits of the field of view. Errors associated with the free surfaces could be minimized by having data sets with more grains and we hope this will be possible in the future. Finally, there are rare events where a grain is divided in two by another (usually a twin). When divided, the grain experiences an apparent large negative volume change that is not the result of the normal grain shrinkage process.

The time interval over which the experiment occurs also plays an important role in our ability predict whether a grain grows or shrinks. Consider, for example, the idealized case where an ensemble of grains continues to grow without stagnation. The average grain size increases continuously until the end point is reached when the entire sample is made up of one grain. The so-called solid state crystal conversion process is a real world approximation of this ideal situation [45,46]. At any point in time while the average grain size increases, some fraction of all grains can be classified as growing. However, before the endpoint is

reached, all grains other than the one left at the end must eventually shrink and disappear. In other words, while all grains can be classified as shrinking or growing at any instant in time, some growing grains must become shrinking grains given sufficient time. In the current experiment, the total volume changes were, on average, 15% for each anneal state. Changes in the local neighborhood of the grains that influence both F and $\langle F_{NN} \rangle$ during the time intervals used here are one source of uncertainty in the results. While this uncertainty might be reduced by using smaller time intervals, uncertainties in the accuracy of the volume measurement will at some point become influential.

Dake et al. [29] recently reported grain rotation during liquid phase sintering. While we observed no such systematic rotations, it must also be mentioned that our method of matching the grains in different time steps relied on the similarity of the orientations in the two states. Therefore, rotations of several degrees would have led to an unmatched grain pair and it would not have been detected. The fact we are able to match 88% of the grains, and the unmatched grains are well correlated with the non-overlapping fields of view and the disappearance of small grains (see Fig. 4), suggests that any large rotations, if they occur, are rare. Also, the average disorientation between matched grains in two time steps is on the order of 0.05° (see Fig. 2). This is a measure of the uncertainty in the orientation measurements, so rotations below this limit would not be detected in our experiment. In an earlier analysis of these data, rare changes in nearest neighbor disorientations were explained by singular events rather than grain rotation [34].

The analysis of a twinned microstructure clearly presents challenges. When twins are considered as separate grains, the relationship between ΔV and $F - \langle F_{NN} \rangle$ is not obvious. There are several reasons that twins can complicate the analysis. Considering the large fraction of coherent twins, almost every grain will have at least one twin boundary and these boundaries are likely to be far less mobile than the other boundaries. While beyond the scope of the current paper, in the future we will consider the number of coherent twin boundaries bounding a grain as a parameter to predict the volume change. Another difficulty is that plate shaped twins within a grain can have as few as two neighbors; this likely leads to a negative value of $F - \langle F_{NN} \rangle$. However, if the incoherent segments at the edges of the plate are expanding within the grain, its volume will increase. As an example, Lin et al. [25] showed, using a subset of the data considered here, that when twins nucleate at triple lines to lower the grain boundary energy, they expand in size, even though they have only three neighbors and a negative value of $F - \langle F_{NN} \rangle$. Also, because of the very anisotropic shapes of the twins in 3D, the typical relation between grain size and number of neighbors is not expected to be as regular. For example, in Fig. S7, the standard deviation in each grain size class is much larger in the twinned microstructure compared to the microstructure without twins.

Finally, we should question whether or not the microstructure is in a steady state during the experiment. If we base this only on the distribution of grain sizes for faces, one concludes that they are self-similar (see Figs. S5 and S6). Furthermore, the distribution of grain boundary disorientations is also nearly constant. The only measurable change is an approximately 10% increase in the relative area of grain boundaries with a 60° disorientation (see Fig. S10). While this is consistent with the idea that low energy grain boundaries increase in area with respect to higher energy boundaries, they are eventually expected to reach a steady state [47]. Although the increase in the fraction of twins suggests that the distribution of grain boundaries has not reached a steady state, it should be noted that these boundaries have no influence on the microstructure from which twins have been eliminated and this is the one whose volume changes are best correlated to $F - \langle F_{NN} \rangle$.

5. Conclusions

The shapes and sizes of 2500 grains in a Ni polycrystal were measured at six points in time separated by 30 min anneals at 800 °C. During the experiment, the average grain volume increased by 77%. For the individual time intervals, neither the grain size nor the number of neighbors were useful predictors for the sign of a grain's volume change. However, in microstructures where adjacent twin related domains were merged, the difference between the number of neighbors and the average number of neighbors of the neighboring grains is correlated to the sign of the volume change. The correct sign of the volume change is predicted by this metric 65% of the time. These results show that a grain's local neighborhood is more important in determining its volume change than how it compares to the average characteristics of the entire sample. Volume changes in the twinned microstructures were not well correlated with any of the metrics and this is most likely a result of the high concentration of twins (more than 27% of grain boundary area) and their distinct properties.

Acknowledgements

This work was supported by the National Science Foundation under grant DMR 1628994. Data collection was supported by NSF DMR 1105173. Use of the Advanced Photon Source, an Office of Science User Facility operated for the U.S. Department of Energy (DOE) Office of Science by Argonne National Laboratory, was supported by the U.S. DOE under Contract No. DE-AC02-06CH11357.

Appendix A. Supplementary data

Supplementary data to this article can be found online at https://doi.org/10.1016/j.actamat.2019.01.022.

References

[1] H.V. Atkinson, Theories of normal grain-growth in pure single phase systems, Acta Metall. 36 (1988) 469–491. https://doi.org/10.1016/0001-6160(88)90079-x.
[2] G.S. Rohrer, Influence of interface anisotropy on grain growth and coarsening, Annu. Rev. Mater. Res. 35 (2005) 99–126. https://doi.org/10.1146/annurev.matsci.33.041002.094657.
[3] R.M. German, Coarsening in Sintering: Grain Shape Distribution, Grain Size Distribution, and Grain Growth Kinetics in Solid-Pore Systems, Crit. Rev. Solid State Mater. Sci. 35 (2010) 263–305. https://doi.org/10.1080/10408436.2010.525197.
[4] C.S. Smith, Grain Shapes and other Metallurgical Applications of Topology. Metal Interfaces, American Society for Metals, Cleveland, 1952, pp. 65–133.
[5] M.A. Palmer, V.E. Fradkov, M.E. Glicksman, K. Rajan, Experimental Assesment of the Mullins-Von Neumann Grain-Growth Law, Scripta Metall. Mater. 30 (1994) 633–637. https://doi.org/10.1016/0956-716x(94)90442-1.
[6] W.W. Mullins, 2-Dimensional motion of idealized grain boundaries, J. Appl. Phys. 27 (1956) 900–904.
[7] C.S. Smith, Grains, phases, and interfaces - an interpretation of microstructure, T. Am. I. Min. Met. Eng. 175 (1948) 15–51.
[8] C.S. Smith, Some Elementary Principles of Polycrytalline Microstructure, Metall. Rev. 9 (1964) 1–48. https://doi.org/10.1179/mtlr.1964.9.1.1.
[9] D.A. Aboav, The Arrangement of Grains in a Polycrystal, Metallography 3 (1970) 383–390. https://doi.org/10.1016/0026-0800(70)90038-8.
[10] D. Weaire, Some Remarks on the Arrangement of Grains in a Polycrystal, Metallography 7 (1974) 157–160. https://doi.org/10.1016/0026-0800(74)90004-4.
[11] D.A. Aboav, Arrangement of cells in a net, Metallography 13 (1980) 43–58. https://doi.org/10.1016/0026-0800(80)90021-x.
[12] F.C. Hull, Plane section and spatial characteristics of equiaxed beta-brass grains, Mater. Sci. Technol. 4 (1988) 778–785.
[13] D.J. Rowenhorst, A.C. Lewis, G. Spanos, Three-dimensional analysis of grain topology and interface curvature in a beta-titanium alloy, Acta Mater. 58 (2010) 5511–5519. https://doi.org/10.1016/j.actamat.2010.06.030.
[14] M.N. Kelly, K. Glowinski, N.T. Nuhfer, G.S. Rohrer, The five parameter grain boundary character distribution of alpha-Ti determined from three-dimensional orientation data, Acta Mater. 111 (2016) 22–30. https://doi.org/10.1016/j.actamat.2016.03.029.
[15] T. Liu, S. Xia, B. Zhou, Q. Bai, G.S. Rohrer, Three-dimensional geometrical and

topological characteristics of grains in conventional and grain boundary engineered 316L stainless steel, Micron 109 (2018) 58–70. https://doi.org/10.1016/j.micron.2018.04.002.
[16] D. Zoellner, On the Aboav-Weaire-law for junction limited grain growth in two dimensions, Comput. Mater. Sci. 79 (2013) 759–762. https://doi.org/10.1016/j.commatsci.2013.07.031.
[17] M.P. Anderson, G.S. Grest, D.J. Srolovitz, Computer-simulation of normal grain-growth in 3 dimensions, Philos. Mag. B-Phys. Condens. Matter Stat. Mech. Electron. Opt. Magn. Prop. 59 (1989) 293–329. https://doi.org/10.1080/13642818908220181.
[18] F. Wakai, N. Enomoto, H. Ogawa, Three-dimensional microstructural evolution in ideal grain growth - General statistics, Acta Mater. 48 (2000) 1297–1311. https://doi.org/10.1016/s1359-6454(99)00405-x.
[19] C.E. Krill, L.Q. Chen, Computer simulation of 3-D grain growth using a phase-field model, Acta Mater. 50 (2002) 3057–3073.
[20] X.T. Zhong, D.J. Rowenhorst, H. Beladi, G.S. Rohrer, The five-parameter grain boundary curvature distribution in an austenitic and ferritic steel, Acta Mater. 123 (2017) 136–145. https://doi.org/10.1016/j.actamat.2016.10.030.
[21] U. Lienert, S.F. Li, C.M. Hefferan, J. Lind, R.M. Suter, J.V. Bernier, N.R. Barton, M.C. Brandes, M.J. Mills, M.P. Miller, B. Jakobsen, W. Pantleon, High-energy diffraction microscopy at the advanced photon source, JOM (J. Occup. Med.) 63 (2011) 70–77. https://doi.org/10.1007/s11837-011-0116-0.
[22] G. Johnson, A. King, M.G. Honnicke, J. Marrow, W. Ludwig, X-ray diffraction contrast tomography: a novel technique for three-dimensional grain mapping of polycrystals. II. The combined case, J. Appl. Crystallogr. 41 (2008) 310–318. https://doi.org/10.1107/s0021889808001726.
[23] C.M. Hefferan, J. Lind, S.F. Li, U. Lienert, A.D. Rollett, R.M. Suter, Observation of recovery and recrystallization in high-purity aluminum measured with forward modeling analysis of high-energy diffraction microscopy, Acta Mater. 60 (2012) 4311–4318. https://doi.org/10.1016/j.actamat.2012.04.020.
[24] S.F. Li, J. Lind, C.M. Hefferan, R. Pokharel, U. Lienert, A.D. Rollett, R.M. Suter, Three-dimensional plastic response in polycrystalline copper via near-field high-energy X-ray diffraction microscopy, J. Appl. Crystallogr. 45 (2012) 1098–1108. https://doi.org/10.1107/s0021889812039519.
[25] B. Lin, Y. Jin, C.M. Hefferan, S.F. Li, J. Lind, R.M. Suter, M. Bernacki, N. Bozzolo, A.D. Rollett, G.S. Rohrer, Observation of annealing twin nucleation at triple lines in nickel during grain growth, Acta Mater. 99 (2015) 63–68. https://doi.org/10.1016/j.actamat.2015.07.041.
[26] J. Lind, S.F. Li, R. Pokharel, U. Lienert, A.D. Rollett, R.M. Suter, Tensile twin nucleation events coupled to neighboring slip observed in three dimensions, Acta Mater. 76 (2014) 213–220. https://doi.org/10.1016/j.actamat.2014.04.050.
[27] I.M. McKenna, S.O. Poulsen, E.M. Lauridsen, W. Ludwig, P.W. Voorhees, Grain growth in four dimensions: A comparison between simulation and experiment, Acta Mater. 78 (2014) 125–134. https://doi.org/10.1016/j.actamat.2014.06.028.
[28] J. Sun, A. Lyckegaard, Y.B. Zhang, S.A. Catherine, B.R. Patterson, F. Bachmann, N. Gueninchault, H. Bale, C. Holzner, E. Lauridsen, D.J. Jensen, Iop. 4D Study of Grain Growth in Armco Iron Using Laboratory X-ray Diffraction Contrast Tomography, in: 38th Riso International Symposium on Materials Science, 219, Riso, DENMARK, 2017.
[29] J.M. Dake, J. Oddershede, H.O. Sorensen, T. Werz, J.C. Shatto, K. Uesugi, S. Schmidt, C.E. Krill III., Direct observation of grain rotations during coarsening of a semisolid Al-Cu alloy, Proc. Natl. Acad. Sci. U.S.A. 113 (2016) E5998–E6006. https://doi.org/10.1073/pnas.1602293113.
[30] J. Zhang, Y. Zhang, W. Ludwig, D. Rowenhorst, P.W. Voorhees, H.F. Poulsen, Three-dimensional grain growth in pure iron. Part I. statistics on the grain level, Acta Mater. 156 (2018) 76–85. https://doi.org/10.1016/j.actamat.2018.06.021.
[31] R.D. MacPherson, D.J. Srolovitz, The von Neumann relation generalized to coarsening of three-dimensional microstructures, Nature 446 (2007) 1053–1055. https://doi.org/10.1038/nature05745.
[32] C.M. Hefferan, S.F. Li, J. Lind, U. Lienert, A.D. Rollett, P. Wynblatt, R.M. Suter, Statistics of High Purity Nickel Microstructure From High Energy X-ray Diffraction Microscopy, CMC-Comput. Mat. Contin. 14 (2009) 209–219.
[33] S.F. Li, Imaging of Orientation and Geometry in Microstructures: Development and Applications of High Energy x-ray Diffraction Microscopy. Physics, Carnegie Mellon University, 2011. Ph.D.
[34] C.M. Hefferan, Measurement of Annealing Phenomena in High Purity Metals with Near-field High Energy X-ray Diffraction Microscopy. Physics, Carnegie Mellon Univeristy, 2012. Ph.D.
[35] C.M. Hefferan, S.F. Li, J. Lind, R.M. Suter, Tests of microstructure reconstruction by forward modeling of high energy X-ray diffraction microscopy data, Powder Diffr. 25 (2010) 132–137. https://doi.org/10.1154/1.3427328.
[36] M.A. Groeber, M.A. Jackson, DREAM.3D, A Digital Representation Environment for the Analysis of Microstructure in 3D, Integrating Materials and Manufacturing Innovation 3 (2014) 5.
[37] T. Liu, S. Xia, B. Zhou, Q. Bai, G.S. Rohrer, Three-dimensional study of twin boundaries in conventional and grain boundary-engineered 316L stainless steels, J. Mater. Res. 33 (2018) 1742–1754. https://doi.org/10.1557/jmr.2018.133.
[38] K.G.F. Janssens, D. Olmsted, E.A. Holm, S.M. Foiles, S.J. Plimpton, P.M. Derlet, Computing the mobility of grain boundaries, Nat. Mater. 5 (2006) 124–127.
[39] M. Groeber, S. Ghosh, M.D. Uchic, D.M. Dimiduk, A framework for automated analysis and simulation of 3D polycrystalline micro structures. Part 1: Statistical characterization, Acta Mater. 56 (2008) 1257–1273. https://doi.org/10.1016/j.actamat.2007.11.041.
[40] M. Hillert, On theory of normal and abnormal grain growth, Acta Metall. 13 (1965) 227–238. https://doi.org/10.1016/0001-6160(65)90200-2.
[41] W.W. Mullins, Estimation of the geometrical rate-constant in idealized 3 dimensional grain-growth, Acta Metall. 37 (1989) 2979–2984. https://doi.org/10.1016/0001-6160(89)90333-7.
[42] M.E. Glicksman, P.R. Rios, D.J. Lewis Regular N-hedra, A topological approach for analyzing three-dimensional textured polycrystals, Acta Mater. 55 (2007) 4167–4180. https://doi.org/10.1016/j.actamat.2007.03.014.
[43] J. von Neumann, Discussion - shape of metal grains. Metal interfaces, American Society for Metals Cleveland, OH, 1952, pp. 108–110.
[44] Y.-F. Shen, S. Maddali, D. Menasche, A. Bhattacharya, G.S. Rohrer, R.M. Suter. The Importance of Outliers: A Three Dimensional Study of Grain Growth in α Phase Iron, submitted to Physical Review Materials.
[45] S.J. Dillon, M.P. Harmer, Mechanism of "solid-state" single-crystal conversion in alumina, J. Am. Ceram. Soc. 90 (2007) 993–995. https://doi.org/10.1111/j.1551-2961.2007.01510.x.
[46] S.-J.L. Kang, J.-H. Park, S.-Y. Ko, H.-Y. Lee, Solid-State Conversion of Single Crystals: The Principle and the State-of-the-Art, J. Am. Ceram. Soc. 98 (2015) 347–360. https://doi.org/10.1111/jace.13420.
[47] S.J. Dillon, G.S. Rohrer, Mechanism for the development of anisotropic grain boundary character distributions during normal grain growth, Acta Mater. 57 (2009) 1–7. https://doi.org/10.1016/j.actamat.2008.08.062.